J Neuroimmune Pharmacol (2014) 9:399–412
DOI 10.1007/s11481-014-9532-6

ORIGINAL ARTICLE

An αvβ3 Integrin-Binding Peptide Ameliorates Symptoms of Chronic Progressive Experimental Autoimmune Encephalomyelitis by Alleviating Neuroinflammatory Responses in Mice

Fan Zhang · Jing Yang · Hong Jiang · Shu Han

Received: 22 August 2013 / Accepted: 12 February 2014 / Published online: 28 February 2014

Abstract MOG35-55 triggers chronic, progressive experimental autoimmune encephalomyelitis (EAE) in C57BL/6 mice, and the clinical course of EAE in this model is characterized by macrophage infiltration, axonal demyelination/damage, and progressive paralysis. These stages are usually associated with inflammatory responses in the central nervous system (CNS). This study was designed to investigate the effects of C16, an αvβ3 integrin-binding peptide that targets integrins involved in the transendothelial migration of extravasating inflammatory cells. C16 was applied for only 2 weeks, but the benefits of this therapy lasted at least 8 weeks. Multiple histological and immunohistochemical staining studies, western blotting, enzyme-linked immunosorbent assays, electron microscopy, and cortical somatosensory-evoked potential (c-SEP) electrophysiological tests were employed to assess the degree of inflammation, axonal loss, white matter demyelination, neuronal apoptosis, extent of gliosis, expression of pro-inflammatory cytokines, and functional recovery of differently treated EAE model mice. The results showed that C16 treatment inhibited extensive leukocyte and macrophage accumulation and infiltration, reduced the expression of pro-inflammatory cytokines (tumor necrosis factor-α and interferon-γ), and thereby attenuated and delayed the progression of EAE. Moreover, astrogliosis, demyelination, and axonal and neuronal loss were all alleviated in C16-treated EAE animals, contributing to the improvement of function. These data suggest that the C16 peptide may act as a protective agent by reducing neuroinflammatory responses and improving the microenvironment.

Keywords Multiple sclerosis · Chronic, progressive experimental allergic encephalomyelitis · Inflammatory cell infiltration · Demyelination · Neuroprotective effect

Introduction

Multiple sclerosis (MS) is the most common autoimmune disorder of the central nervous system (CNS). MS affects patients of all ages (Frohman et al. 2006) and has been detected as early as 15 months after birth (Tanoue et al. 2006). MS is characterized by perivascular inflammatory infiltration, demyelination, and axonal loss in the CNS and can follow an acute or chronic disease course (Hassen et al. 2008). Inflammation associated with MS can promote the production of multiple pro-inflammatory cytokines, contributing to the destruction of myelin. Demyelination can then lead to impairment of axons and loss of axonal conduction, which ultimately results in neurodegeneration and permanent disability (Basso et al. 2008; Berard et al. 2010; Soulika et al. 2009).

Animal models of experimental autoimmune encephalomyelitis (EAE) play an important role in identifying and elucidating several aspects of MS biology, including inflammation, immune surveillance, and immune-mediated tissue injury (Denic et al. 2011). Integrins are the molecular limbs of a cell, enabling the trafficking and entry of pathogenic leukocytes into inflamed tissues (Kanwar et al. 2000). In the EAE model, circulating leukocytes enter the CNS, producing inflammation and myelin/axon damage (Berard et al. 2010; Cervellini et al. 2013; Denic et al. 2011). Previous studies showed that an antibody against α4

Electronic supplementary material The online version of this article (doi:10.1007/s11481-014-9532-6) contains supplementary material, which is available to authorized users.

F. Zhang · J. Yang · S. Han (✉)
Institute of Anatomy and Cell Biology, Medical College, Zhejiang University, 866 Yuhangtang Road, Hangzhou 310058, China
e-mail: han00shu@zju.edu.cn

H. Jiang
Department of Electrophysiology, Sir Run Run Shaw Hospital, Medical College, Zhejiang University, Hangzhou, China

integrin prevented leukocyte infiltration and suppressed the clinical and pathological features of acute EAE (Cervellini et al. 2013). Moreover, an antibody directly targeting mucosal address in cell adhesion molecule-1 (MAdCAM-1), the preferential ligand for α4β7, also effectively prevented the development of a progressive, non-remitting form of EAE (Kanwar et al. 2000). In addition to the above-mentioned integrins, integrin αvβ3, which has been shown to be upregulated in autoimmune T cells (Roy et al. 2007), was also shown to modulate leukocyte adhesion to intercellular adhesion molecule-1 (ICAM-1) and enable leukocytes to migrate effectively across the endothelium (Weerasinghe et al. 1998). The synthetic C16 peptide (KAFDITYVRLKF) represents a functional laminin domain and selectively binds to αvβ3 integrin, interferes with leukocyte ligands required for transmigration, and competitively blocks the transmigration of leukocytes attempting to enter the CNS (Han et al. 2010). Importantly, the C16 peptide is not immunosuppressant and does not affect systemic leukocyte counts (Han et al. 2010). We recently tested the impact of C16 in an acute EAE model induced by guinea pig spinal cord homogenate (GPSCH) in Lewis rats (Fang et al. 2013). During the early phase of MS development (9–14 days), C16 reduced the transendothelial migration of C8166-CD4 lymphoblast cells and alleviated the extensive infiltration of leukocytes and macrophages in the CNS (Fang et al. 2013). However, this acute model did not allow us to test the impact of C16 on advanced manifestations of the MS disease, including the extensive axonal damage resulting from demyelination (Basso et al. 2008; Berard et al. 2010; Soulika et al. 2009).

In the present study, we tested C16 in a well-established chronic model of EAE elicited in C57BL/6 mice by immunization with myelin oligodendrocyte glycoprotein peptide 35–55 (MOG peptide) (Berard et al. 2010; Ransohoff 2012). This peptide induces axonal vacuolization and fragmentation typical of late-stage chronic MS, thereby providing a good model to investigate the mechanistic relationship between the CNS immune milieu (continuing inflammation) and myelin/axonal loss (Berard et al. 2010; Denic et al. 2011). This chronic EAE model also exhibits pathological features typical of chronic, progressive MS, in which the lasting inflammation (chemokine/cytokine expression) and myelin loss gradually aggravate axonal lesions (Berard et al. 2010).

In the current study, we sought to identify the effects of the C16 peptide on MS by starting treatment early in the course of the disease and monitoring the animals over a period of 8 weeks.

Materials and Methods

Animals and EAE Induction

In total, 80 eight-week-old female C57BL/6 mice (25–30 g) were obtained from Zhejiang University Laboratory Animal Services Centre. Of these mice, eight were used as normal controls, and the remaining 72 were randomly assigned into the vehicle-treated control group (n=18) and three C16 treatment groups (n=54, 18 mice per group). Experiments were conducted in accordance with the NIH Guidelines for the Care and Use of Laboratory Animals, with approval from the animal ethics committee at Zhejiang University.

Chronic EAE was elicited in vehicle-treated control mice and C16-treated mice using the MOG35-55 peptide and pertussis toxin (PTx) as previously described (Yin et al. 2010). In brief, each animal was immunized subcutaneously in the flank with 200 μg of MOG35-55 peptide (MEVGWYRSPFSRVVHLYRNGK; synthesized by Shanghai Science Peptide Biological Technology Co., Ltd, China) emulsified in complete Freund's adjuvant (CFA) containing 500 μg of heat-killed *Mycobacterium tuberculosis*. Immediately thereafter, and again 24 h later, the mice received an intraperitoneal injection of PTx (300 ng/100 μL phosphate-buffered saline [PBS]). The animals were examined daily for disability. Clinical scores were defined as follows (Yin et al. 2010): 0, no signs; 1, tail tonicity loss; 2, flaccid tail; 3, ataxia and/or paresis of hindlimbs; 4, complete paralysis of hindlimbs; 5, moribund or death. The disability scores were obtained daily over the course of the 8-week experiment by researchers blinded to the treatment of the animals until the time of sacrifice.

Intravenous Injection of C16

The C16 peptide was prepared and administered as previously described (Fang et al. 2013). In brief, C16 (KAFDITYVRLKF) was dissolved in distilled water with 0.3 % acetic acid. The solution was sterilized through a 0.22-μm disc filter and then neutralized with NaOH to pH 7.4. This solution was buffered by adding an equal volume of sterile PBS, and the final stock solution was adjusted to a concentration of 2 mg/mL. The animals receiving C16 were divided into three groups: low-dose (0.1 mg/day, n=18), medium-dose (0.2 mg/day, n=18), and high-dose (0.4 mg/day, n=18). Mice in each group received 0.2 mL of C16 solution of different concentrations. The control (vehicle) group (n=18) was treated with 0.2 mL of the same solvent without the peptide via intravenous injection of the tail vein. The first dose was given immediately after EAE induction (following the MOG35-55 injection and PTx injection), and thereafter, the solutions were injected intravenously each day for a period of 2 weeks.

Neurophysiological Testing

Cortical somatosensory evoked potentials (c-SEP) were recorded at 2 and 8 weeks after immunization for six mice in each group. The heads of the mice were placed in a stereotaxic frame under sodium pentobarbital anesthesia (60 mg/kg i.p.), and loss of eye blink and withdrawal reflexes were observed

to assess anesthesia depth. An incision was made in the median sagittal plane to remove the overlying fascia and muscles from the skull. Two burr holes were drilled for placement of cortical and reference electrodes using stereotaxic coordinates. For registration of c-SEP, screw electrodes were implanted over the primary somatosensory cortical areas, and cerebellar reference electrodes were placed over the appropriate cortical area. A pair of needle electrodes was inserted in each of the hind limbs to stimulate the tibial nerve. Positive current pulses of 0.2-mA magnitude and 200-μs duration at a frequency of 1 Hz were used for limb stimulation. Signals were digitally converted and stored for post-hoc analysis. At the end of the recordings, the skull was carefully cleaned and the skin closed with surgical sutures. The values obtained by the three series of stimulations were processed by statistical analyses. The peak positive and negative values were measured, and the results are expressed as the mean ± SEM for voltage amplitude (μV) and latency (ms) (All et al. 2009; Devaux et al. 2003; Troncoso et al. 2000, 2004).

Perfusion and Tissue Collection and Processing

Animals in the vehicle control and C16 treatment groups were sacrificed at 2 and 8 weeks after immunization (six mice per time point in each group). Brain cortical and spinal tissues were collected, and sections were prepared as previously described (Fang et al. 2011). A portion of each tissue was processed for histological assessment, immunohistological staining, and immunofluorescent staining. The remaining tissues were fixed in 2.5 % glutaraldehyde solution and then examined by transmission electron microscopy.

Histology Assessment

We employed hematoxylin and eosin (H&E) staining and cresyl violet (Nissl) staining to assess inflammation and neuron survival, respectively. Inflammation was scored as follows (Ma et al. 2010): 0, no inflammation; 1, cellular infiltrates only around blood vessel and meninges; 2, mild cellular infiltrates in parenchyma with 1–10 per section; 3, moderate cellular infiltrates in parenchyma with 11–100 per section; and 4, serious cellular infiltrates in parenchyma with more than 100 per section. Neuron counts from both spinal cord anterior horns were performed and restricted to neurons with a well-defined nucleolus and a cell body with adequate amounts of endoplasmic reticulum. Digital images were collected using a Nikon TE-300 microscope in three visual fields/per section with 200× magnification under bright-field viewing.

Luxol fast blue (LFB) staining was used to evaluate the degree of axon demyelination, as previously described (Fang et al. 2011). Demyelination was scored as follows (Yin et al. 2010): 0, normal white matter; 1, rare foci; 2, a few areas of demyelination; 3, confluent perivascular or subpial demyelination; 4, massive perivascular and subpial demyelination involving one half of the spinal cord with presence of cellular infiltrates in the CNS parenchyma; and 5, extensive perivascular and subpial demyelination involving the whole cord section with presence of cellular infiltrates in the CNS parenchyma. Neuron counts and digital images were processed as previously described (Fang et al. 2011).

Bielschowsky silver staining was performed as described previously to estimate axonal loss (Fang et al. 2011). Axonal loss was assessed using the following scale (Yin et al. 2010): 0, no axonal loss; 1, a few foci of superficial axonal loss involving less than 25 % of the tissue; 2, foci of deep axonal loss that encompassed over 25 % of the tissue; and 3, diffuse and widespread axonal loss.

Immunohistochemical Staining

The tissue sections were subjected to immunohistochemical staining with polyclonal rabbit anti-CD4 (1:500; Abcam, Cambridge, MA, USA), anti-CD45 (1:200; Abcam), anti-CD68/ED1 (1:200; Santa Cruz Biotechnology, Santa Cruz, CA, USA), anti-tumor necrosis factor alpha (TNF-α, 1:1000; ProSci Inc., CA, USA), anti-caspase 3 (1:500; Cayman Chemical, Ann Arbor, MI, USA), anti-160 KD neurofilament M (NF-M; 1:1000; Neuromics, MN, USA), and mouse anti-myelin basic protein (MBP, 1:500, Abcam) antibodies. Immunohistochemical staining was performed as described previously (Fang et al. 2011). Primary antibody omission controls were used to confirm the specificity of the immunohistochemical labeling. The CD4+, CD45+, and CD68+ cells were counted under 400× magnification (field radius = 225 μm), and Image Pro Plus acquisition software (Media Cybernetics, Silver Spring, MD) was used to evaluate positively labeled cells in three visual fields per Section. A quantitative analysis to compare the number of infiltrating leukocytes, lymphocytes, and macrophages was also performed.

Immunofluorescence Staining

The sections were incubated with primary polyclonal rabbit anti-glial fibrillary acidic protein (GFAP, 1:200; Thermo Fisher Scientific, Waltham, MA, USA). Immunofluorescence staining was performed as previously described (Fang et al. 2011). Primary antibody omission controls were used to confirm the specificity of the immunohistochemical labeling. Areas showing immunoreactivity for GFAP were analyzed with NIH Image software.

Processing for Electron Microscopy

Tissues fixed with 2.5 % glutaraldehyde were washed three times with 0.1 M phosphate buffer (PB). Post-fixed tissues were placed in 1 % osmium tetroxide at 4 °C overnight and

then washed three times with 0.1 M PB. Processing for electron microscopy was performed as described previously (Fang et al. 2011). Images were captured first at low resolution and then at higher magnification in different regions of the white matter.

Cytokine Quantification by Enzyme-Linked Immunosorbent Assay (ELISA)

Peripheral blood samples were collected from mice that had been sacrificed by decapitation at 2 weeks and 8 weeks post-immunization (n=3 mice per time point in each group). Plasma samples were collected on ice via centrifugation (20 min at 1,000×g within 30 min of collection and then at 10,000×g for 10 min at 4 °C for complete platelet removal) using heparin as an anticoagulant. All samples were aliquoted and stored at −80 °C. To assess cytokine expression, plasma samples were incubated in 96-well plates pre-coated with antibodies to IFN-γ (BioLegend Inc., San Diego, CA, USA) and TNF-α (R&D Systems, Minneapolis, MN, USA) at 37 °C for 60 min. Horseradish peroxidase (HRP)-conjugated goat anti-rabbit IgG (Bio-Rad, Hercules, CA, USA) diluted 1:2000 was used as the secondary antibody. The optical density was measured at 450 nm on a Model 680 Microplate Reader (Bio-Rad Laboratories, Corston, UK). Optical density readings were analyzed using GraphPad Prism 4 (GraphPad Software, Inc.).

Western Blotting

Mice were sacrificed by decapitation at 2 and 8 weeks post-immunization (n=3 mice per time point in each group). The whole brain cortex and a 10-mm lumbar spinal cord segment from each animal were prepared for western blotting with primary rabbit polyclonal anti-GFAP (1:500), anti-TNF-α (1:2000), anti-NF-M (1:2000; Neuromics), and anti-caspase 3 (1:500) antibodies. Western blotting was performed as described previously (Troncoso et al. 2004). To normalize protein bands to a loading control, membranes were washed in Tris-buffered saline with Tween 20 (TBST) and re-probed with rabbit anti-β-actin antibodies (1:5000; Abcam) followed by incubation with peroxidase-conjugated goat anti-rabbit antibodies (1:5000; Santa Cruz) and ECL detection. For the negative control, the primary antibody was omitted.

Statistical Analysis

All statistical graphs were created in GraphPad Prism software version 4.0. Kruskal–Wallis nonparametric analysis was conducted followed by a non-parametric Mann–Whitney test on each pair of data. Data were analyzed by SPSS 13.0 software, and $P<0.05$ was considered statistically significant.

Results

C16 Reduced the Clinical Symptoms of EAE in Mice

In vehicle-treated mice, disease symptoms appeared on days 6–9 after immunization and peaked (paralysis) at week 2 after immunization. The maximal score (maximum severity of disease in an individual mouse) of vehicle-treated EAE mice was 3.0±0.5 (Fig. 1a–c). During the remission/progressive phase, the clinical scores of vehicle-treated EAE mice remained high (2.2±3.6). In general, animals treated with different doses of C16 showed a disease course similar to that of the vehicle group, but the disease progression was dramatically delayed, and the peak stage was postponed until 18–21 days after immunization. Additionally, the disease severity at each time point was decreased (Fig. 1a–c). The maximal scores were also reduced in C16-treated EAE mice (2±0.3, Fig. 1c). No differences were observed among C16-treated groups. However, at the time of peak clinical score in the C16-treated groups, only the medium (0.2 mg/day) and high (0.4 mg/day) dose groups were significantly different from the vehicle-treated group, whereas the low-dose (0.1 mg/day) group was not different from the vehicle-treated group.

C16 Treatment Reduced Inflammation in the CNS

The chronic EAE model was generally characterized by a gradual perivascular accumulation of inflammatory cells within the cortex and spinal cord, reaching peak intensity 2 weeks after immunization. Immunostaining showed that leukocytes stained positively for the pan-leukocyte marker CD45, and sub-classes including CD4+ T-helper lymphocytes and CD68+ macrophages were infiltrating cells detectable in the CNS. Our data demonstrated that widespread perivascular and parenchymal infiltration of leukocytes, lymphocytes, and extravasated macrophages occurred in the CNS of vehicle-treated control mice but was significantly reduced by consecutive intravenous C16 treatment (Supplementary Fig. 1i–l). A quantitative analysis indicated that C16 treatment significantly reduced T lymphocyte (CD4+) infiltration, leukocyte (CD45+) extravasation, and macrophage (CD68+) activation in both tissue types in a dose-dependent manner (Supplementary Fig. 1q–t, supplementary Fig. 2). At week 8 after immunization, the extent of infiltration in the vehicle control was lower than that after 2 weeks, but "perivascular cuffing" infiltration was still evident (Supplementary Fig. 1c, g, k). Medium and high doses of C16 also significantly suppressed inflammatory cell infiltration in the CNS at this late stage of EAE (Supplementary Fig. 1, 2). Mice treated with the highest dose of C16 maintained near-normal levels of all inflammatory cell types at both time points, even though daily treatments were only provided during the first 2 weeks. Western blot analysis confirmed that the protein expression level of CD4 was elevated in

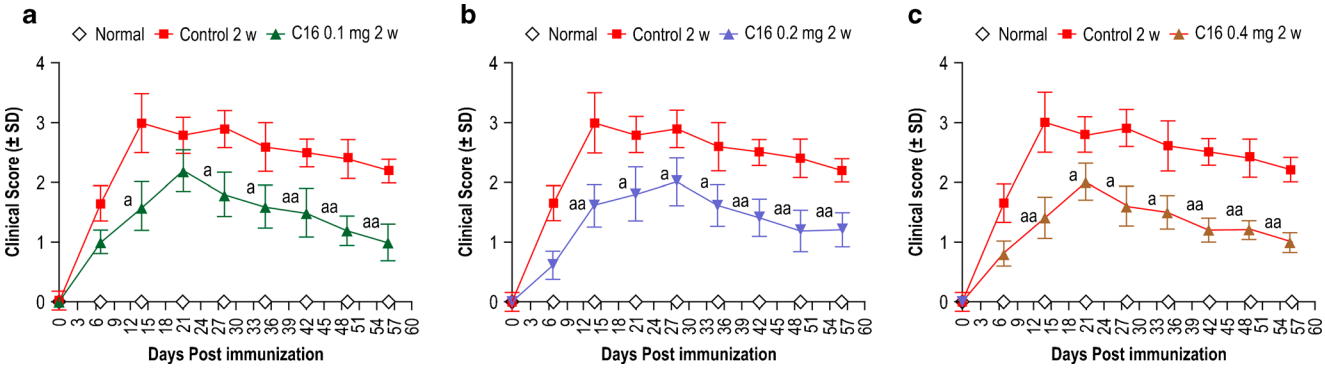

Fig. 1 Clinical progression of EAE was attenuated after low- (**a**), medium- (**b**), and high-dose C16 (**c**) treatment as measured by disease score, but no differences in effects were observed among C16-treated groups. *a*, $P<0.05$ versus the vehicle-treated group at the same time point. *aa*, $P<0.01$ versus the vehicle-treated group at the same time point

vehicle-treated mice but reduced by C16 (Supplementary Fig. 3). Altogether, these data suggest that C16 treatment initiated early in the development of EAE efficiently suppressed CNS inflammation during the 8-week study period.

C16 Treatment Suppressed the Expression of Pro-Inflammatory TNF-α and IFN-γ

Immunohistochemical labeling revealed abundant expression of TNF-α in neurons and other neural cells in the CNS of vehicle control-treated EAE mice. Treatment with the medium and high doses of C16 resulted in significantly fewer TNF-α-immunoreactive neuronal cells when compared with the vehicle-treated and low-dose C16-treated groups (Supplementary Fig. 4a–h). The western blot analysis showed that at early (week 2) and late (week 8) stages of the clinical course, upregulation of TNF-α occurred in the brain cortex and spinal cord of vehicle control-treated EAE mice, whereas a marked decrease in TNF-α expression was observed in each of the C16-treated groups (Supplementary Fig. 4k–p). Next, we measured the expression

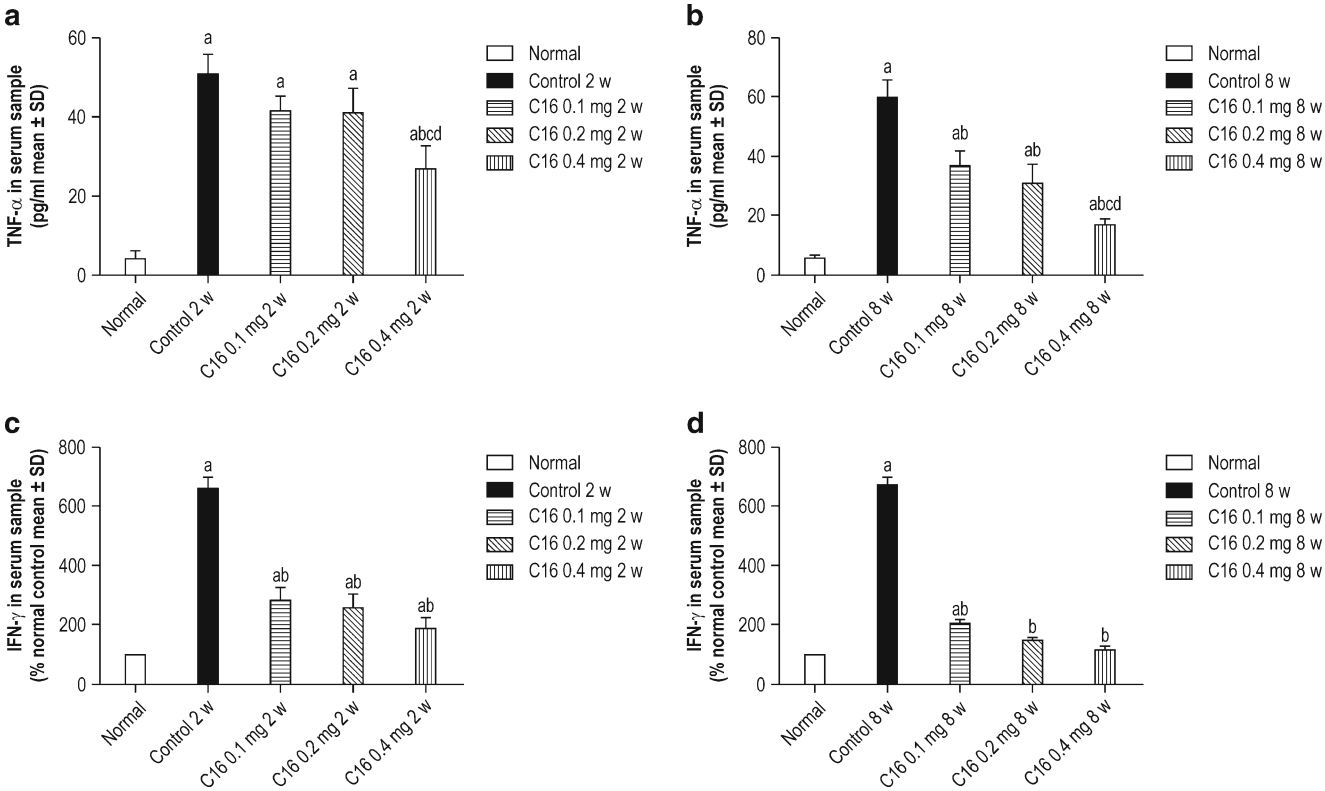

Fig. 2 **a**, **b** C16 treatment suppressed the expression of the pro-inflammatory cytokine TNF-α. The level of TNF-α expression was measured by ELISA. *a*, $P<0.05$ versus the normal control; *b*, $P<0.05$ versus vehicle-treated EAE mice; *c*, $P<0.05$ versus 0.1 mg/day C16-treated EAE mice; *d*, $P<0.05$ versus 0.2 mg/day C16-treated EAE mice. **c**, **d** The expression of IFN-γ was measured at weeks 2 (**c**) and 8 (**d**) after treatment with C16 by ELISA. *a*, $P<0.05$ versus the normal control; *b*, $P<0.05$ versus vehicle-treated EAE mice

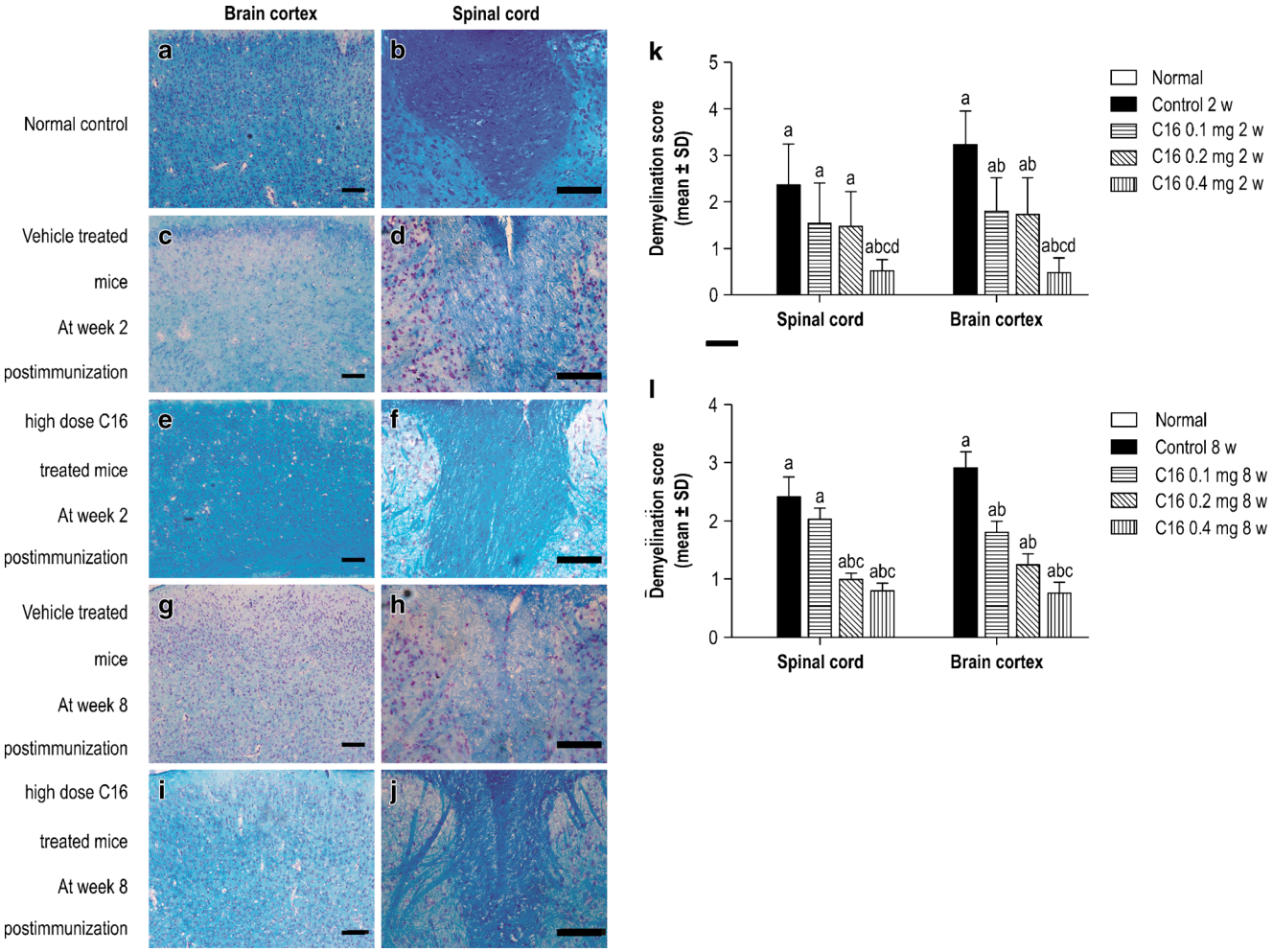

Fig. 3 C16 treatment inhibited demyelination in the CNS. Demyelination was measured by Luxol fast blue staining with counterstaining by cresyl violet. **a**, **c**, **e**, **g**, **i** Coronal sections of the motor cortex; **b**, **d**, **f**, **h**, **j** traverse sections through the posterior column of the lumbar spinal cord; bar = 100 μm. At week 2 after immunization: **a**, **b** normal animal control; **c**, **d** vehicle-treated EAE mice; **e**, **f** high-dose C16-treated EAE mice. At week 8 after immunization: **g**, **h** vehicle-treated EAE mice; **i**, **j** high-dose C16-treated EAE mice: **k**, **l** Demyelization was measured by the estimated demyelination score. *a*, $P<0.05$ versus the normal control; *b*, $P<0.05$ versus vehicle-treated mice; *c*, $P<0.05$ versus 0.1 mg/per day C16-treated EAE mice; *d*, $P<0.05$ versus 0.2 mg/day C16-treated EAE mice

levels of TNF-α and IFN-γ in the blood serum by ELISA. C16 application noticeably reduced the expression of both IFN-γ and TNF-α, which were significantly upregulated in vehicle-treated EAE mice (Fig. 2). Altogether, these data show that C16 efficiently reduced inflammation in the CNS and that this effect persisted at least 6 weeks after cessation of the treatment.

C16 Treatment Inhibited Demyelination and Prevented Axon Loss

Because chronic inflammation causes axonal damage, we evaluated whether the anti-inflammatory effects of C16 reduce or prevent axon demyelination. We used two methods to quantify demyelination: demyelination scores based on myelin staining by LFB (Fig. 3) and myelination area based on MBP immunostaining (Supplementary Fig. 5). Massive perivascular infiltration and adjacent demyelinated areas were present in the brain and spinal cord parenchyma of vehicle-treated EAE mice at the peak time of the disease course (week 2 after immunization; Fig. 3c, d; Supplementary Fig. 5a, b). At the same time point, when treated with different doses of the C16 peptide, the confluent areas of demyelination were reduced (Fig. 3, Supplementary Fig. 5). In the high-dose C16-treated group, only rare foci of demyelination were found (Fig. 3e, f; Supplementary Fig. 5e, f). The vehicle control mice exhibited more severe demyelination at 8 weeks after immunization than after 2 weeks (Fig. 3g, h; Supplementary Fig. 5c, d). The highest dose of C16 completely preserved myelination at both time points (Fig. 3i, j; Supplementary Fig. 5g, h).

Furthermore, treatment with medium- and high-dose C16 markedly reduced axonal damage. The impact of C16 treatment on axonal loss was quantified by immunostaining of the

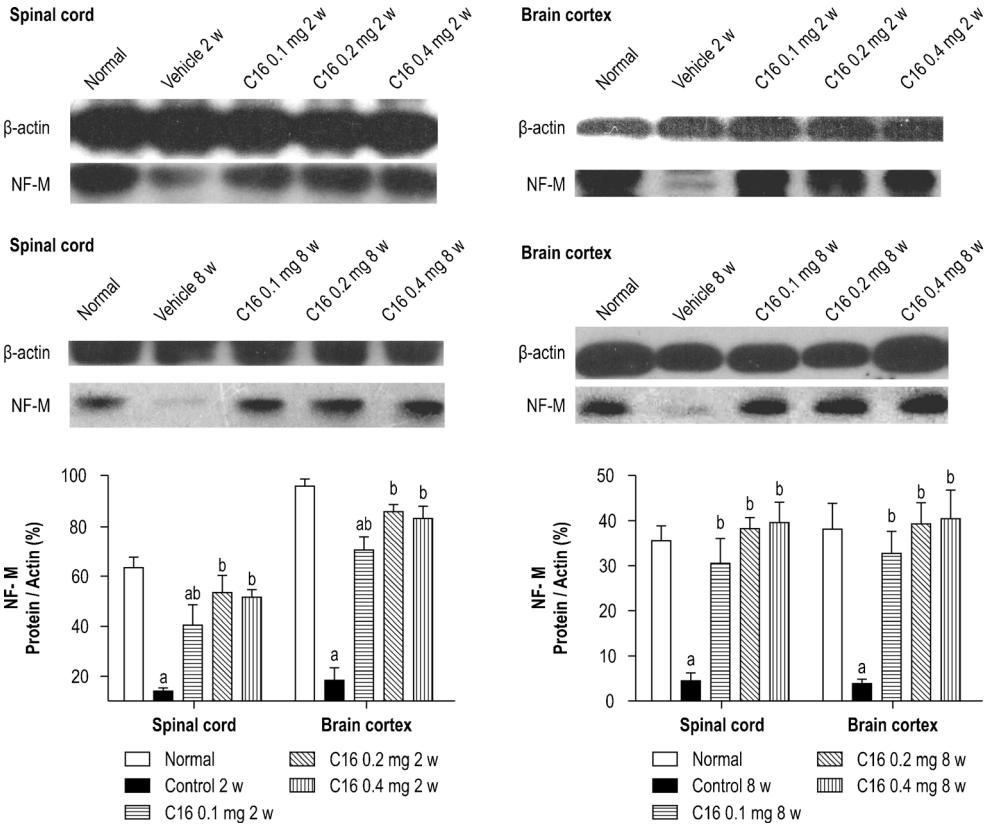

Fig. 4 C16 treatment prevented axonal loss. NF-M expression decreased markedly in both the spinal cord and cerebral cortex following EAE induction. This effect was reversed after treatment with C16 relative to the vehicle-treated control at weeks 2 and 8 after immunization, as shown by western blotting. *a*, $P<0.05$ versus the normal control; *b*, $P<0.05$ versus vehicle-treated EAE mice

neurofilament NF-M and confirmed by Bielschowsky staining of CNS white and gray matter. Vehicle-treated mice exhibited widespread axonal loss at both 2 (Supplementary Fig. 6b) and 8 (Supplementary Fig. 6f) weeks after immunization. Low-dose C16 increased perikaryal and axonal NF-M immunostaining in motor neuron filaments (Supplementary Fig. 6c, g). The motor neurons of medium- and high-dose C16-treated mice presented abundant perikaryal NF-M immunoreactivity and high NF-M positive axon density (Supplementary Fig. 6b, e, h, l). Quantitative analysis indicated that C-16 increased NF-M immunostaining and alleviated neuronal atrophy at both time points (Fig. 6k, l). These data were supported by the western blot analysis of NF-M expression in the vehicle control compared to C16-treated animals (Fig. 4).

Bielschowsky staining revealed visible axonal loss in the white and gray matter of the CNS in vehicle-treated EAE mice. Deteriorating axonal loss appeared at week 8 after immunization (Supplementary Fig. 7c, d). In low-dose C16-treated EAE mice, axons were also undergoing gradual loss, and the injured axons exhibited swelling, deformation, and ovoid formation (Supplementary Fig. 7e–h). A much higher number of axons with relatively normal formation was preserved in C16-treated EAE mice (Supplementary Fig. 7i–p).

Transmission electron microscopy was performed to further identify myelin sheath splitting and vacuolated changes and to examine potential signs of apoptosis in the vehicle control group. Severe edema and leakage of inflammatory cells from the blood vessels were detected in the extracellular space surrounding the vessels (Fig. 5d). The neurons of the EAE vehicle control mice showed signs of apoptosis, including shrunken nuclei with condensed, fragmented, and marginated nuclear chromatin (Fig. 5e). More lightly vacuolated myelin sheaths were found in each of the C16-treated EAE groups, and the corresponding axons and neighboring nuclei presented relatively normal ultrastructure (Fig. 5f–i). At week 8 after immunization in the vehicle control group, some myelin lamellae were still undergoing vesicular disintegration, and some were undergoing remyelination (Fig. 5j). Additionally, more remyelinated fibers appeared in high-dose C16-treated EAE mice (Fig. 5l).

C16 Treatment Inhibited Apoptosis and Reduced Neuronal Death

Signs of apoptosis, as initially identified by electron microscopy analysis of the spinal cord and brain tissue, were verified by measuring the expression level of caspase-3, an enzyme involved in the execution of the mammalian apoptotic pathway for programmed cell death. Western blot analysis also revealed a significant increase in active caspase-3 expression in the vehicle control from weeks 2 to 8 after immunization; this effect was significantly reversed by C16 treatment, especially in the high-dose group (Supplementary Fig. 8). A marked increase in the number of caspase-3-immunoreactive

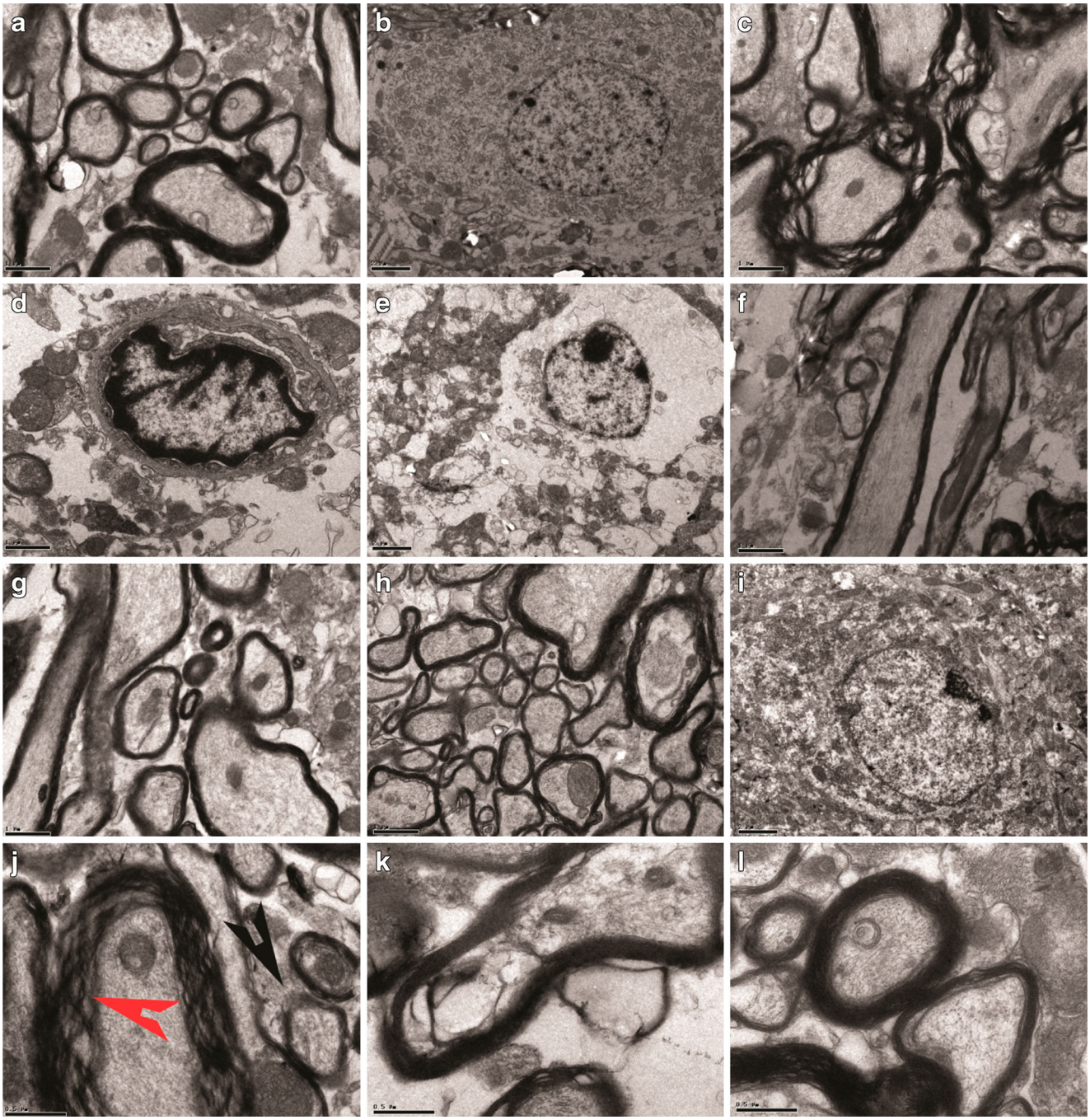

Fig. 5 Electron micrographs demonstrating the prevention of demyelination or axonal loss and inhibition of neuronal apoptosis by C16 treatment. **a**, **b** Normal control group. **a** Normal myelinated axons exhibited dark ring-shaped myelin sheaths surrounding the axon. **b** Normal nuclei of neurons with uncondensed chromatin. **c**–**e** Vehicle-treated EAE rats at week 2 after immunization. A considerable amount of the myelin sheath displayed splitting, vacuoles, and loose and fused changes, and axons were shrunken and dissolving (**c**). Severe leakage out of the blood vessels and tissue edema was detected in the extracellular space surrounding the vessels (**d**). The neurons of the vehicle control showed apoptotic signs of shrunken nuclei with condensed, fragmented, and marginated nuclear chromatin (**e**). The low- (**f**), medium- (**g**), and high-dose C16-treated (**h**) groups exhibited more lightly vacuolated myelin sheaths. The neighboring nuclei (**i**) of C16-treated mice resembled the normal ultrastructure. At week 8 after immunization in the vehicle control group, demyelination (*red arrow*) and remyelination (*black arrow*) simultaneously appeared in vehicle-treated EAE mice (**j**). Additionally, more remyelinated fibers appeared in high-dose (0.4 mg/day) C16-treated (**l**) mice than in in low-dose (0.1 mg/day) C16-treated (**k**) mice. a, c, d, f, g, h: bar = 1 μm; b, e, i: bar = 2 μm; j, k, l: bar = 0.5 μm

neuronal cells in the spinal cords and motor cortices of vehicle-treated EAE rats was accompanied by severe inflammation and loss of neurons (Supplementary Fig. 8), especially in the late stage of the clinical course (week 8 after

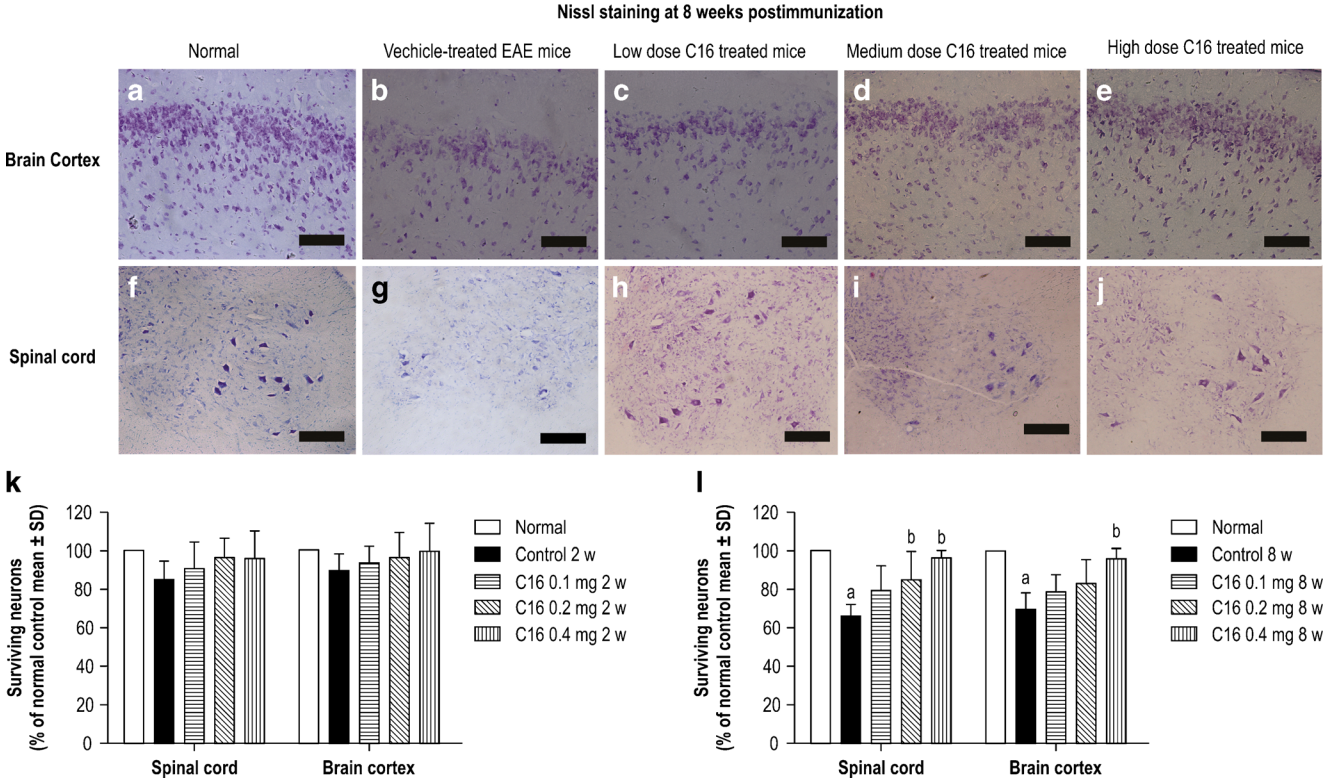

Fig. 6 Treatment with C16 reduced the loss of neurons both in the spinal cord and brain. Nissl staining, bar = 100 μm (**a**–**e**), coronal sections of the brain motor cortex; **f**–**j** traverse sections through the anterior horn of the lumbar spinal cord. At week 8 after immunization: **a**, **f** normal mice; **b**, **g** vehicle-treated EAE mice; **c**, **h** low-dose C16-treated EAE mice; **d**, **i** medium-dose C16-treated EAE mice; **e**, **j** high-dose C16-treated EAE mice. Surviving neural cells (each group is presented as a % of the normal control) in different groups at weeks 2 (**k**) and 8 (**l**) after immunization, calculated after Nissl staining. *a*, $P<0.05$ versus the normal control; *b*, $P<0.05$ versus vehicle-treated EAE rats

immunization). Compared with the vehicle control, C16 treatment, especially in the high-dose group, significantly reduced caspase-3 IR-positive neural cell numbers at both weeks 2 and 8 after immunization (Supplementary Fig. 8).

Thus, remarkable neuron loss was observed in the anterior horn of the spinal cord and motor cortex of the vehicle-treated EAE rats at both weeks 2 and 8 after immunization (Fig. 6b, g) when compared with normal animals (Fig. 6a, f). However, the high-dose C16 treatment significantly reduced neuronal loss in the CNS (Fig. 6).

C16 Suppressed Reactive Astrocyte Proliferation and Reactive Astrogliosis

During chronic CNS inflammation, astrocytes become activated (reactive) and proliferate, leading to astrogliosis (glial scarring). To assess the effects of treatment with vehicle and C16 on EAE-induced reactive gliosis, we examined the expression of GFAP, a marker for astrocytes, by western blot analysis and immunofluorescence labeling. Immunolabeling showed that astrocytes proliferated and reactive gliosis occurred in the CNS of vehicle-treated mice (Fig. 7b) at week 2 after immunization, and obvious glial scarring emerged at week 8 after immunization (Fig. 7c). GFAP expression and astrocyte proliferation were significantly reduced in C16-treated groups (Fig. 7). Western blot analysis revealed that the expression of GFAP increased in both the spinal cord and cerebral cortex of vehicle-treated EAE mice and that GFAP expression levels were significantly decreased in each C16-treated group (Fig. 7). Thus, these data demonstrated that long-term C16 treatment was able to reverse glial scarring in the chronic EAE model.

C16 Reversed MOG-Induced Electrophysiological Dysfunction

In general, delayed latency of c-SEP indicates the severity of demyelination, and a decrease in amplitude indicates the extent of axonal damage. EAE induction resulted in an increase in the latency to waveform initiation, a decrease in peak amplitude (Table 1), and a decrease in the waveform slope in vehicle-treated mice (Fig. 8). However, intravenous injection of medium- and high-dose C16 peptide, starting at immunization and continuing for 2 weeks, significantly prevented electrophysiological disturbances and reversed the disease-related N-P latency delays. C16 treatment also resulted in variations in the peak-to-peak decrease of c-SEP amplitude between negative deflection N and positive deflection P, both

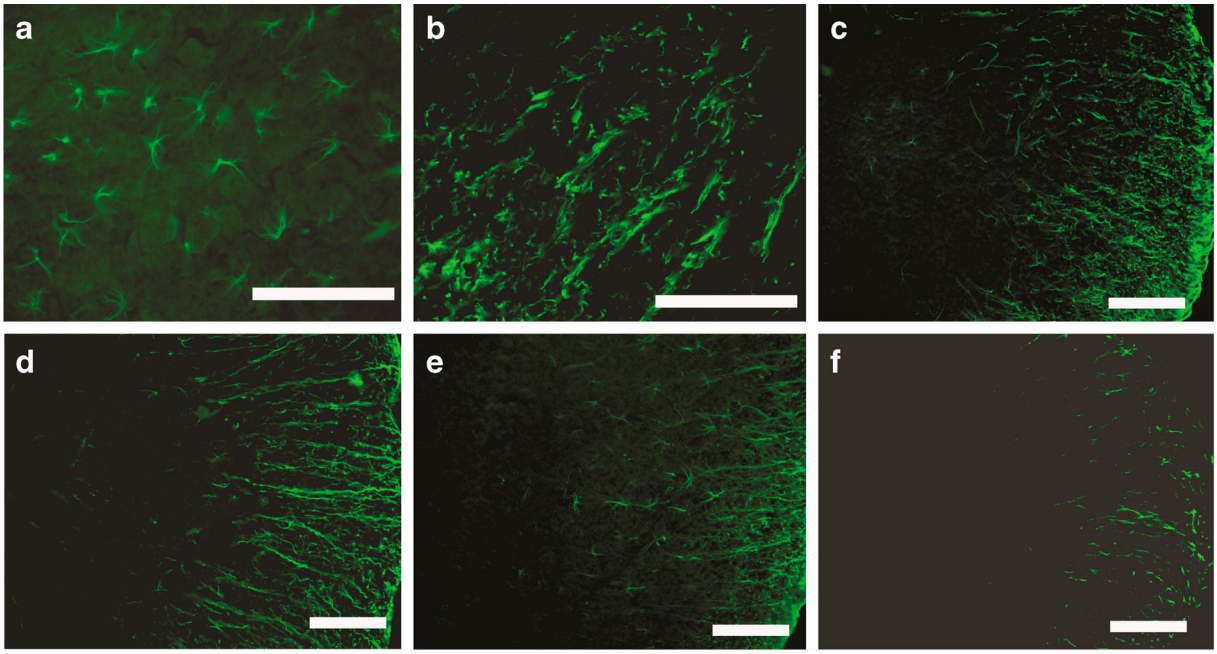
a
b
c
d
e
f

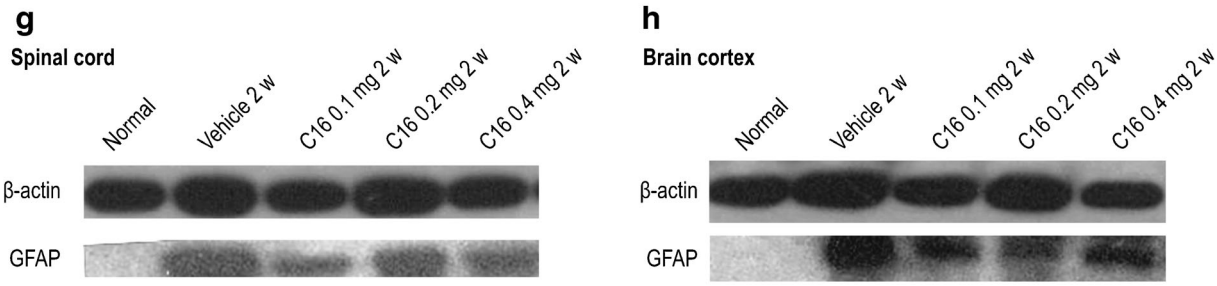
g
Spinal cord
Normal
Vehicle 2 w
C16 0.1 mg 2 w
C16 0.2 mg 2 w
C16 0.4 mg 2 w
β-actin
GFAP
h
Brain cortex
Normal
Vehicle 2 w
C16 0.1 mg 2 w
C16 0.2 mg 2 w
C16 0.4 mg 2 w
β-actin
GFAP

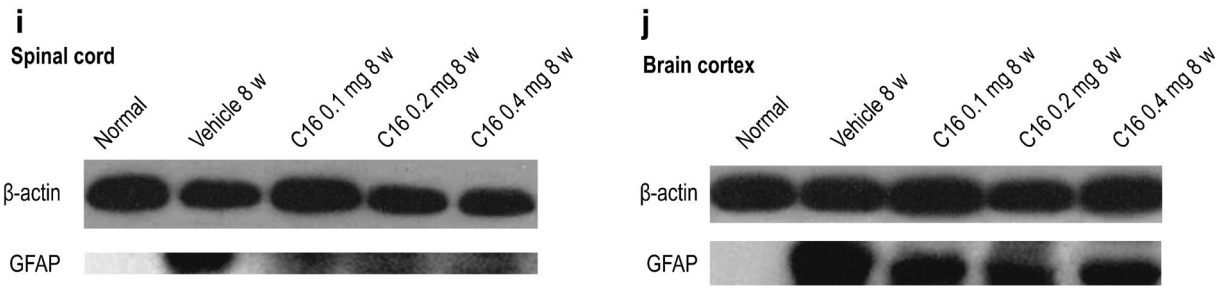
i
Spinal cord
Normal
Vehicle 8 w
C16 0.1 mg 8 w
C16 0.2 mg 8 w
C16 0.4 mg 8 w
β-actin
GFAP
j
Brain cortex
Normal
Vehicle 8 w
C16 0.1 mg 8 w
C16 0.2 mg 8 w
C16 0.4 mg 8 w
β-actin
GFAP

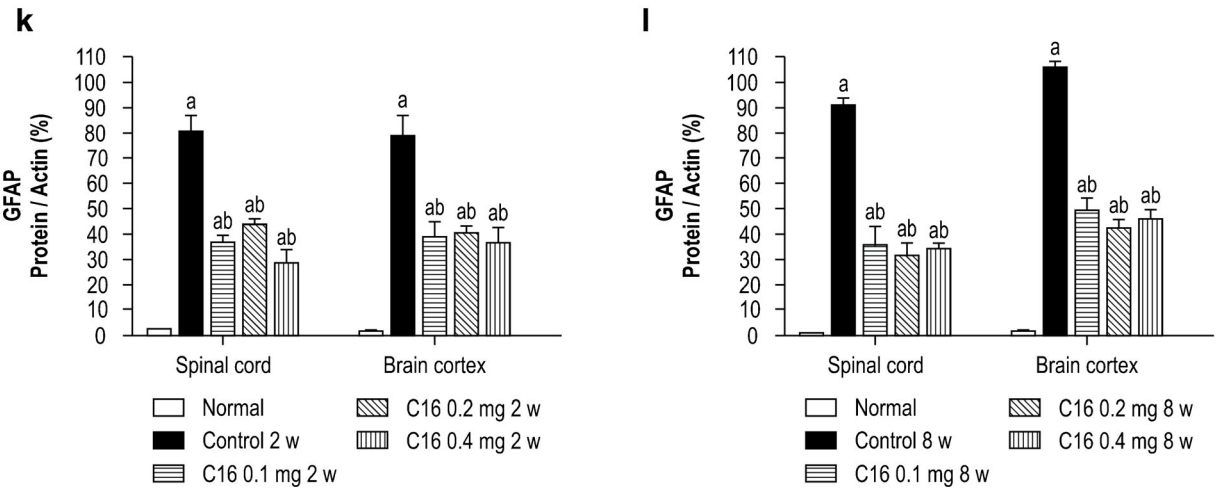
k
GFAP
Protein / Actin (%)
110
100
90
80
70
60
50
40
30
20
10
0
a
ab
ab
ab
a
ab
ab
ab
Spinal cord
Brain cortex
Normal
Control 2 w
C16 0.1 mg 2 w
C16 0.2 mg 2 w
C16 0.4 mg 2 w
l
GFAP
Protein / Actin (%)
110
100
90
80
70
60
50
40
30
20
10
0
a
ab
ab
ab
a
ab
ab
ab
Spinal cord
Brain cortex
Normal
Control 8 w
C16 0.1 mg 8 w
C16 0.2 mg 8 w
C16 0.4 mg 8 w

◀ **Fig. 7** Treatment with C16 inhibited reactive gliosis. FITC-conjugated GFAP immunofluorescent staining (transverse sections through the lateral column of the lumbar spinal cord) was used. At week 8 after immunization, vehicle-treated EAE mice (**c**) and low-dose C16-treated EAE mice (**d**) exhibited evidence of glial scar formation, whereas reactive gliosis was markedly decreased in medium- (**e**) and high-dose C16-treated (**f**) EAE mice. Astrocytes were normally shaped in the CNS of normal mice (**a**) and a glial scar was formed by reactivated astroglia in the CNS of EAE mice (**b**). **g–l** C16 suppressed the proliferation of reactive astrocytes and reduced reactive gliosis. The level of GFAP expression increased in the CNS of vehicle-treated EAE mice but obviously decreased in mice treated with C16, as shown by western blotting. *a* $P<0.05$ versus the normal control; *b* $P<0.05$ versus vehicle-treated EAE mice

in the acute (week 2) and chronic (week 8) stages of the disease (Fig. 8a, b).

Discussion

Upon immunization with MOG35-55, C57BL/6 mice develop a chronic non-remitting paralytic disease (Dore-Duffy et al. 2011; Murugesan et al. 2012; Slavin et al. 1998). Histologically, MOG-induced EAE in C57BL/6 mice shares characteristics with MS such as extensive axonal injury, marked demyelination, and mononuclear cell infiltration (Cervellini et al. 2013). Chronic inflammation is associated with perivascular extravasation of CD45+ leukocytes, indicating an ongoing progressive inflammatory process. This early influx of macrophages and CD68-labeled active microglia is believed to maintain the pathological process, as CD4 is commonly expressed on the surface of T-helper lymphocytes and can mediate inflammatory autoimmune disease in the central nervous system (Arnold and Hagg 2011; Mensah-Brown et al. 2011). The extravasated leukocytes also infiltrate the parenchyma and white matter (Slavin et al. 1998), which could significantly augment CNS inflammation and lead to widespread CNS damage (Bettini et al. 2009). Previous studies have shown that general reduction of the infiltration of such cells improves tissue sparing and function in rodents (Mangas et al. 2008). Therefore, in the current study, we used mice to establish a model of EAE and to subsequently investigate the effects of the C16 peptide in this model.

The C16 peptide can recognize and bind to $\alpha v\beta 3$, which plays an important role in leukocyte accumulation and adhesion processes (Weerasinghe et al. 1998; Han et al. 2010), and can then competitively block transmigration of leukocytes attempting to cross the endothelium (Fang et al. 2013). In agreement with this mechanism, our study demonstrates widespread perivascular and parenchymal infiltration of leukocytes, lymphocytes (labeled by the pan-leukocyte marker CD45 and the lymphocyte marker CD4), and activated microglia. Extravasated macrophages (labeled by CD68) appeared in the CNS of vehicle-treated control mice but were significantly reduced by consecutive intravenous C16 treatment. Inflammatory scores were clearly reduced in mice treated with different doses of C16 relative to mice treated with the vehicle control. An obvious decrease in CD4 expression in the CNS was also detected in C16-treated groups. Because CD4+ T cells can increase disease severity and induce sustained inflammation of the CNS (Slavin et al. 1998), the absence of CD4+ T cells in the C16-treated groups may have dramatically reduced the damage caused by inflammation.

Inflammation leads to the production of IFN-γ, TNF-α, and other proteases; induces the infiltration of inflammatory cells into the CNS; contributes to the destruction of myelin; and eventually causes injury to axons (Garay et al. 2008; Ghezzi and Mennini 2001). Our results show that application of C16 noticeably reduced the expression of TNF-α and IFN-γ when compared with vehicle-treated control EAE

Table 1 C16 treatment reduced the c-SEP latencies and increased c-SEP amplitudes

Groups	Latency (ms)		
	N	*P*	Wave amplitude (μV mean ± SD)
2 W			
Normal	9.35±0.7	14.25±1.63	10.29±3.27
Vehicle	37.5±0.29	44.05±0.35	2.95±0.9
0.1 mg C16	25.5±0.57	30±1.27	2.8±1.56
0.2 mg C16	20.5±1.56	24.4±1.7	3.27±0.73
0.4 mg C16	15.65±0.35	23.4±3.11	6.93±2.55 **
8 W			
Normal	9.58±0.21	14.65±1.58	13.55±4.17
Vehicle	36.2±0.14	43.1±0.42	2.75±1.34
0.1 mg C16	24.6±0.95	32.2±1.87	3.12±0.79*
0.2 mg C16	20.63±0.38	27.93±1.64	6.62±1.40 **
0.4 mg C16	16.2±2.26	21.93±3.32	13.40±3.60 **

*$P<0.05$ versus vehicle-treated EAE mice; **$P<0.01$ versus vehicle-treated EAE mice

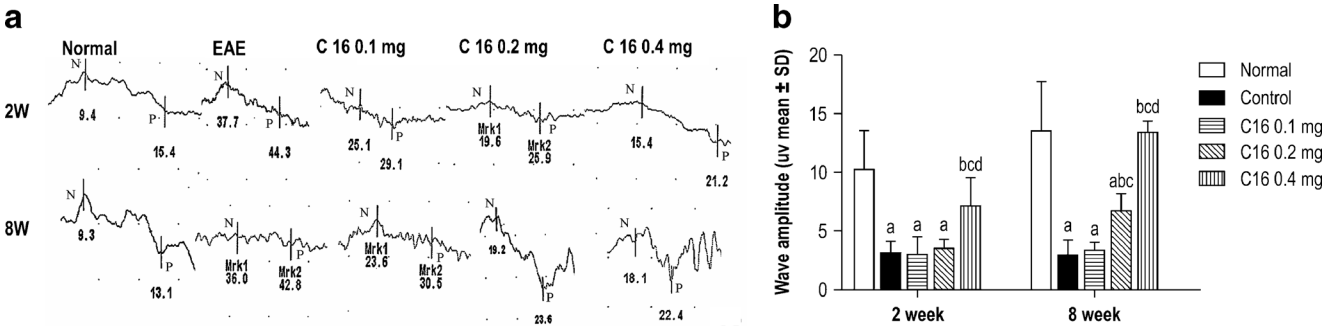

Fig. 8 C16 reduced the clinical severity of EAE in mice. EAE induction was measured by determining the somatosensory-evoked potential (c-SEP) latencies and amplitudes (measured from peak to peak between negative deflection N and positive deflection P). **a** Waveform of c-SEP. **b** c-SEP amplitude. *a*, $P<0.05$ versus the normal control; *b*, $P<0.05$ versus vehicle-treated EAE mice; *c*, $P<0.05$ versus 0.1 mg/day C16-treated EAE mice; *d*, $P<0.05$ versus 0.2 mg/day C16-treated EAE mice

mice, possibly because C16 treatment blocked the accumulation and infiltration of inflammatory cells, resulting in a gradual decrease in the amount of pro-inflammatory factors.

Extensive demyelination and loss of MBP immunoreactivity were observed in our vehicle control-treated mice, revealing an inflammation-related loss of myelinated fibers. Axonal loss following demyelination is strongly related to reduced motor coordination (McGavern et al. 2000). We presumed that improvement of the microenvironment in C16-treated EAE mice would alleviate secondary injury. Indeed, a significant decrease of demyelination areas and reduction of axonal damage were detected in C16-treated groups at both weeks 2 and 8 after immunization. The observation of more myelinated axons under electron microscopy in C16-treated groups further confirmed the protective effects of C16 on myelin and axons. All of these phenomena may be ascribed to a reduction in the inflammatory milieu.

The CNS is vulnerable to demyelination and axonal damage, resulting in conduction deficits that reflect overt functional loss. In electrophysiological tests, impaired nerve impulses can be quantified by the amplitude and latency of c-SEP responses to sensory stimuli (Balatoni et al. 2007). Delayed latency is more indicative of focal demyelination, whereas a decrease in amplitude indicates the extent of axonal damage (Balatoni et al. 2007; Merrill et al. 2009). A previous study also suggested that increased latency is correlated with increased disease severity and decreased SEP amplitude related to the appearance and severity of clinical symptoms (Balatoni et al. 2007). Our results indicate that in the vehicle-treated EAE mice, simulative induction resulted in a prolongation of c-SEP latency and a significant peak-to-peak reduction in c-SEP amplitude from the N to P wave, suggestive of demyelination and axonal injury in the spinal cord dorsal column, which was consistent with the results of histological examinations. In medium- and high-dose C16-treated groups, C16 application significantly reversed the reduction in waveform amplitude and the waveform slope seen in vehicle-treated EAE animals and prevented the increase in latency. We hypothesized that these effects of C16 were possibly mediated by reduced inflammatory damage to myelin and inhibition of axonal degeneration (Balatoni et al. 2007; Merrill et al. 2009).

Increasing evidence indicates that astrogliosis plays two contradictory roles in the pathogenesis of demyelinating disease (Nair et al. 2008; Voskuhl et al. 2009; Xu et al. 2006). On the one hand, proliferated astrocytes form perivascular barriers that restrict the influx of leukocytes into the CNS parenchyma (Voskuhl et al. 2009). On the other hand, upon exposure to the inflammatory milieu, astrocytes become activated astrocytes, which can promote immune-mediated demyelination by priming autoreactive T cells and expressing cytokines, including TNF-α, nitric oxide (NO), and interleukin-1β (IL-1β) (Pifarre et al. 2011; Xu et al. 2006). Chronically activated astrocytes are believed to contribute to the development of MS (Xu and Drew 2007). Astrocytes respond to insult with a process of cellular activation known as reactive astrogliosis, and are thus key players in driving CNS inflammation; they have been directly implicated in the pathophysiology of EAE (Brambilla et al. 2014). Astrocyte products could be toxic to host CNS cells, including myelin-producing oligodendrocytes and neurons (Pifarre et al. 2011; Xu et al. 2006; Xu and Drew 2007). Therefore, agents that block the activation of astrocytes may be effective in the treatment of MS. Our results showed that the astrocyte proliferation and glial scar formation that visibly appeared in the vehicle-treated control group were reduced by C16 treatment, possibly because of improvement of the regional microenvironment and reduction of activated astrocytes; therefore, this therapy may be useful for relieving disability in locomotor function.

It is generally accepted that the association between cell death and tissue damage results from immune system activation and subsequent inflammation. In the development and progression of diseases, elevation of intracellular neurotoxic cytokines can induce neuronal apoptosis through multiple mechanisms (Crowe et al. 1997; Liu et al. 1997). Direct neurotoxic injury to neurons and trans-synaptic damage caused by inflammatory attack on the axons may contribute

to the pathology (Shu et al. 2011; Tegla et al. 2009). Furthermore, whereas remyelination is the most critical process for remission, myelin-forming oligodendrocytes are important targets of the immune attack (Tegla et al. 2009). At chronic stages of neuro-inflammation, many oligodendrocytes undergo apoptosis (Profyris et al. 2004; Warden et al. 2001), leading to denudement of axons and deterioration of axonal conduction, thereby exacerbating the impediment of function (Profyris et al. 2004). In the present study, the improved microenvironment reduced the release of neurotoxic cytokines, further suppressing neuronal and oligodendrocytic apoptosis, which may have led to more rapid recovery of locomotor function in our C16-treated mice.

In our study, both low- and high-dose groups showed a similar effect in terms of the mean clinical score, especially at later stages of the disease course (4–8 weeks after immunization). All the C16 dosage groups showed their maximum scores around 2 at 21 days after injection, while the maximum score of vehicle control was 14 days after immunization, indicating that C16 treatment postponed the onset of motor symptoms. At the time of the peak clinical score in the C16-treated groups, only the medium (0.2 mg/per day)- and high (0.4 mg/per day)-dose C16-treated groups were significantly different from the vehicle-treated group, which may underlie the improved c-SEP responses in the medium- and high-dose C16-treated groups in the early stage. In the late stage, similar clinical score curves of all three C16 groups was in accordance with the improved c-SEP responses in all three groups.

Although C16 treatment was only performed for 2 weeks duration, a clear reduction in disease severity was also detected at week 8 after immunization. These results imply that C16 treatment had a long-lasting effect on symptom reduction in EAE and that C16 may act as a protective agent against neuroinflammatory disease by improving the microenvironment in the CNS (Arnold and Hagg 2011). Because we chose the C16 dosage based on previous work in a mouse spinal cord injury model (Han et al. 2010) and the results did not exhibit clear dose-dependent effects, a lower concentration of the peptide should be included in subsequent studies to identify the lowest effective dosage of C16 in EAE treatment.

Acknowledgments This work was funded by the Zhejiang Provincial Natural Science Foundation of China no. R2110025 and the National Natural Science Foundation of China, project no. 81271333.

Conflict of Interest The authors declare that they have no conflicts of interest.

References

All AH, Walczak P, Agrawal G, Gorelik M, Lee C, Thakor NV, Bulte JW, Kerr DA (2009) Effect of MOG sensitization on somatosensory evoked potential in Lewis rats. J Neurol Sci 284:81–89

Arnold SA, Hagg T (2011) Anti-inflammatory treatments during the chronic phase of spinal cord injury improve locomotor function in adult mice. J Neurotrauma 28:1995–2002

Balatoni B, Storch MK, Swoboda EM, Schönborn V, Koziel A, Lambrou GN, Hiestand PC, Weissert R, Foster CA (2007) FTY720 sustains and restores neuronal function in the DA rat model of MOG-induced experimental autoimmune encephalomyelitis. Brain Res Bull 74: 307–316

Basso AS, Frenkel D, Quintana FJ, Costa-Pinto FA, Petrovic-Stojkovic S, Puckett L, Monsonego A, Bar-Shir A, Engel Y, Gozin M, Weiner HL (2008) Reversal of axonal loss and disability in a mouse model of progressive multiple sclerosis. J Clin Invest 118:1532–1543

Berard JL, Wolak K, Fournier S, David S (2010) Characterization of relapsing-remitting and chronic forms of experimental autoimmune encephalomyelitis in C57BL/6 mice. Glia 58:434–445

Bettini M, Rosenthal K, Evavold BD (2009) Pathogenic MOG-reactive CD8+ T cells require MOG-reactive CD4+ T cells for sustained CNS inflammation during chronic EAE. J Neuroimmunol 213:60–68

Brambilla R, Morton PD, Ashbaugh JJ, Karmally S, Lambertsen KL, Bethea JR (2014) Astrocytes play a key role in EAE pathophysiology by orchestrating in the CNS the inflammatory response of resident and peripheral immune cells and by suppressing remyelination. Glia 62:452–467

Cervellini I, Ghezzi P, Mengozzi M (2013) Therapeutic efficacy of erythropoietin in experimental autoimmune encephalomyelitis in mice, a model of multiple sclerosis. Methods Mol Biol 982:163–173

Crowe MJ, Bresnahan JC, Shuman SL, Masters JN, Beattie MS (1997) Apoptosis and delayed degeneration after spinal cord injury in rats and monkeys. Nat Med 3:73–76

Denic A, Johnson AJ, Bieber AJ, Warrington AE, Rodriguez M, Pirko I (2011) The relevance of animal models in multiple sclerosis research. Pathophysiology 18:21–29

Devaux J, Forni C, Beeton C, Barbaria J, Béraud E, Gola M, Crest M (2003) Myelin basic protein-reactive T cells induce conduction failure in vivo but not in vitro. Neuroreport 14:317–320

Dore-Duffy P, Wencel M, Katyshev V, Cleary K (2011) Chronic mild hypoxia ameliorates chronic inflammatory activity in myelin oligodendrocyte glycoprotein (MOG) peptide induced experimental autoimmune encephalomyelitis (EAE). Adv Exp Med Biol 701:165–173

Fang M, Huang JY, Wang J, Ling SC, Rudd JA, Hu ZY, Xu LH, Yuan ZG, Han S (2011) The anti-neuroinflamatory and neurotrophic effects of combined therapy with Annexin II and Reg-2 on injured spinal cord. Neurosignals 19:16–43

Fang M, Sun Y, Hu Z, Yang J, Davies H, Wang B, Ling S, Han S (2013) C16 peptide shown to prevent leukocyte infiltration and alleviate detrimental inflammation in acute allergic encephalomyelitis model. Neuropharmacology 70C:83–99

Frohman EM, Racke MK, Raine CS (2006) Multiple sclerosis–the plaque and its pathogenesis. N Engl J Med 10:942–955

Garay L, Gonzalez Deniselle MC, Gierman L, Meyer M, Lima A, Roig P, De Nicola AF (2008) Steroid protection in the experimental autoimmune encephalomyelitis model of multiple sclerosis. Neuroimmunomodulation 15:76–83

Ghezzi P, Mennini T (2001) Tumor necrosis factor and motoneuronal degeneration: an open problem. Neuroimmunomodulation 9:178–182

Han S, Arnold SA, Sithu SD, Mahoney ET, Geralds JT, Tran P, Benton RL, Maddie MA, D'Souza SE, Whittemore SR, Hagg T (2010) Rescuing vasculature with intravenous angiopoietin-1 and alpha v beta 3 integrin peptide is protective after spinal cord injury. Brain 133:1026–1042

Hassen GW, Feliberti J, Kesner L, Stracher A, Mokhtarian F (2008) Prevention of axonal injury using calpain inhibitor in chronic

progressive experimental autoimmune encephalomyelitis. Brain Res 1236:206–215

Kanwar JR, Kanwar RK, Wang D, Krissansen GW (2000) Prevention of a chronic progressive form of experimental autoimmune encephalomyelitis by an antibody against mucosal addressin cell adhesion molecule-1, given early in the course of disease progression. Immunol Cell Biol 78:641–645

Liu XZ, Xu XM, Hu R, Du C, Zhang SX, McDonald JW, Dong HX, Wu YJ, Fan GS, Jacquin MF, Hsu CY, Choi DW (1997) Neuronal and glial apoptosis after traumatic spinal cord injury. J Neurosci 17: 5395–5406

Ma X, Jiang Y, Wu A, Chen X, Pi R, Liu M, Liu Y (2010) Berberine attenuates experimental autoimmune encephalomyelitis in C57 BL/6 mice. PLoS One 5:e13489

Mangas A, Coveñas R, Bodet D, de León M, Duleu S, Geffard M (2008) Evaluation of the effects of a new drug candidate (GEMSP) in a chronic EAE model. Int J Biol Sci 4:150–160

McGavern DB, Murray PD, Rivera-Quiñones C, Schmelzer JD, Low PA, Rodriguez M (2000) Axonal loss results in spinal cord atrophy, electrophysiological abnormalities and neurological deficits following demyelination in a chronic inflammatory model of multiple sclerosis. Brain 123:519–531

Mensah-Brown EP, Shahin A, Al Shamisi M, Lukic ML (2011) Early influx of macrophages determines susceptibility to experimental allergic encephalomyelitis in Dark Agouti (DA) rats. J Neuroimmunol 232:68–74

Merrill JE, Hanak S, Pu SF, Liang J, Dang C, Iglesias-Bregna D, Harvey B, Zhu B, McMonagle-Strucko K (2009) Teriflunomide reduces behavioral, electrophysiological, and histopathological deficits in the Dark Agouti rat model of experimental autoimmune encephalomyelitis. J Neurol 256:89–103

Murugesan N, Paul D, Lemire Y, Shrestha B, Ge S, Pachter JS (2012) Active induction of experimental autoimmune encephalomyelitis by MOG35-55 peptide immunization is associated with differential responses in separate compartments of the choroid plexus. Fluids Barriers CNS 9:15

Nair A, Frederick TJ, Miller SD (2008) Astrocytes in multiple sclerosis: a product of their environment. Cell Mol Life Sci 65:2702–2720

Pifarre P, Prado J, Baltrons MA, Giralt M, Gabarro P, Feinstein DL, Hidalgo J, Garcia A (2011) Sildenafil (Viagra) ameliorates clinical symptoms and neuropathology in a mouse model of multiple sclerosis. Acta Neuropathol 121:499–508

Profyris C, Cheema SS, Zang D, Azari MF, Boyle K, Petratos S (2004) Degenerative and regenerative mechanisms governing spinal cord injury. Neurobiol Dis 15:415–436

Ransohoff RM (2012) Animal models of multiple sclerosis: the good, the bad and the bottom line. Nat Neurosci 15:1074–1077

Roy A, Liu X, Pahan K (2007) Myelin basic protein-primed T cells induce neurotrophins in glial cells via alphavbeta3 integrin. J Biol Chem 282:32222–32232

Shu Y, Yang Y, Qiu W, Lu Z, Li Y, Bao J, Feng M, Hu X (2011) Neuroprotection by ulinastatin in experimental autoimmune encephalomyelitis. Neurochem Res 36:1969–1977

Slavin A, Ewing C, Liu J, Ichikawa M, Slavin J, Bernard CC (1998) Induction of a multiple sclerosis-like disease in mice with an immunodominantepitope of myelin oligodendrocyte glycoprotein. Autoimmunity 28:109–120

Soulika AM, Lee E, McCauley E, Miers L, Bannerman P, Pleasure D (2009) Initiation and progression of axonopathy in experimental autoimmune encephalomyelitis. J Neurosci 29:14965–14979

Tanoue K, Yamashita S, Masuko K, Osaka J, Iai M, Yamada M (2006) Two cases of acute disseminated encephalomyelitis which occurred before the age of 24 months. No To Hattatsu 38:363–367

Tegla CA, Cudrici C, Rus V, Ito T, Vlaicu S, Singh A, Rus H (2009) Neuroprotective effects of the complement terminal pathway during demyelination: implications for oligodendrocyte survival. J Neuroimmunol 213:3–11

Troncoso E, Muller D, Czellar S, Zoltan Kiss J (2000) Epicranial sensory evoked potential recordings for repeated assessment of cortical functions in mice. J Neurosci Methods 97:51–58

Troncoso E, Muller D, Korodi K, Steimer T, Welker E, Kiss JZ (2004) Recovery of evoked potentials, metabolic activity and behavior in a mouse model of somatosensory cortex lesion: role of the neural cell adhesion molecule (NCAM). Cereb Cortex 14:332–341

Voskuhl RR, Peterson RS, Song B, Ao Y, Morales LB, Tiwari-Woodruff S, Sofroniew MV (2009) Reactive astrocytes form scar-like perivascular barriers to leukocytes during adaptive immune inflammation of the CNS. J Neurosci 29:11511–11522

Warden P, Bamber NI, Li H, Esposito A, Ahmad KA, Hsu CY, Xu XM (2001) Delayed glial cell death following Wallerian degeneration in white matter tracts after spinal cord dorsal column cordotomy in adult rats. Exp Neurol 168:213–224

Weerasinghe D, McHugh KP, Ross FP, Brown EJ, Gisler RH, Imhof BA (1998) A role for the alphavbeta3 integrin in the transmigration of monocytes. J Cell Biol 142:595–607

Xu J, Drew PD (2007) Peroxisome proliferator-activated receptor-gamma agonists suppress the production of IL-12 family cytokines by activated glia. J Immunol 178:1904–1913

Xu J, Chavis JA, Racke MK, Drew PD (2006) Peroxisome proliferator-activated receptor-alpha and retinoid X receptor agonists inhibit inflammatory responses of astrocytes. J Neuroimmunol 176:95–105

Yin JX, Tu JL, Lin HJ, Shi FD, Liu RL, Zhao CB, Coons SW, Kuniyoshi S, Shi J (2010) Centrally administered pertussis toxin inhibits microglia migration to the spinal cord and prevents dissemination of disease in an EAE mouse model. PLoS One 5:e12400